



# DEM-aided direct shear testing of granular sands incorporating realistic particle shape

Yu Zhou<sup>1</sup> · Huabin Wang<sup>1</sup> · Bo Zhou<sup>1</sup> · Jianmei Li<sup>1</sup>

Received: 19 July 2017 / Published online: 28 July 2018  
© Springer-Verlag GmbH Germany, part of Springer Nature 2018

## Abstract

Discrete element method (DEM) of granular sands incorporating the effect of the realistic particle shape has been an important issue for many years. In this context, this study proposed a novel framework for the generation of realistic-shaped particles of natural sands in 3D DEM simulations. The generation framework mainly included micro-CT ( $\mu$ CT) scanning of sand particles, image processing of  $\mu$ CT images, spherical harmonic reconstruction of the particle surface, and clump generation by the overlapping multisphere clump method (OMCM) in DEM simulations. To validate the accuracy of OMCM, the volume and inertia moment of the clump were carefully investigated, and a set of optimized generation parameters was then determined to ensure the accuracy of the clump and the limit number of the filling spheres. Based on the generation framework, a clump sample with realistic particle shapes and a corresponding sphere sample were generated to conduct a series of direct shear testing. The simulation results demonstrated that the realistic particle shape highly increases the particle interlocking rather than the anisotropic intensity of strong contact force chains, and in turn enhances the shear resistance and the shear-induced dilation of the sands. It was also found that the inter-particle contacts of the clump sample have higher friction mobilization than that of the sphere sample, which identified the micromechanism of the shape effect on the particle interlocking.

**Keywords** Particle shape · Spherical harmonic reconstruction · Overlapping multisphere clump method · Direct element method

## 1 Introduction

Particle shape, in terms of general form and surface texture, has been widely acknowledged to play a significant role in determining the mechanical properties of natural sands. In the last three decades, a large number of experimental studies have found that general form and surface texture, respectively, enhance particle interlocking and inter-particle friction, producing an increase in shear strength and shear-induced dilation of sands [1, 2]. As an alternative, the discrete element method (DEM) has also made a significant contribution towards elucidating the micromechanical mechanisms of the particle shape effect on the mechanical properties of sands [3–6]. In this context, it is essential to take the particle shape effect into account when conducting DEM studies of natural sands.

In order to consider the particle shape effect in DEM studies, two major methods have been commonly used by researchers. The first method is to introduce a rheology-type rolling resistance model to define the constitutive relationship of inter-particle contact, which is capable of reflecting the anti-rotation effect between the contacted particles induced by the particle shape [7–9]. As compared to the rolling resistance model, a more direct method to reflect the particle shape effect is to incorporate irregular particle shapes into DEM simulations. In this regard, a number of modelling techniques have been proposed in the extant literature, including ellipsoids [3, 5], polyhedrons [10–12], spherocylinders [13], and potential particles [14, 15]. However, these methods are only capable of generating idealized and repetitive particle shapes within a particle assembly. According to the basic understanding of natural sands, shapes of the component particles are totally random and distinct from each other. Determining how to incorporate the effect of realistic particle shapes of natural sands into DEM studies remains a major challenge.

Recently, the development of X-ray micro-computed tomography ( $\mu$ CT) technology has provided a powerful

✉ Bo Zhou  
zhoubohust@hust.edu.cn

<sup>1</sup> Department of Civil Engineering and Mechanics, Huazhong University of Science and Technology, Wuhan 430074, China

tool for the 3D visualization and characterization of the microstructure and micromorphology of natural sand particles [16–20]. The authors have made a comprehensive study on the particle shape of natural sands by using image analysis and spherical harmonic (SH) analysis based on  $\mu$ CT images of natural sands [17–19]. Therefore, the application of  $\mu$ CT technology constitutes a feasible approach for researchers to incorporate realistic particle shapes of natural sands into DEM simulations. For example, based on  $\mu$ CT images, Andrade and colleagues used the granular element method (GEM) [21, 22], an advanced DEM combined with non-uniform rational basis splines, to capture complex particle shapes of natural sands. However, the complicated detection of inter-particle contacts always resulted in huge computation cost of the GEM simulations. Consequently, a simpler and more efficient method, named the multisphere clump method (MCM), has been widely utilized in conventional DEM frameworks, which creates complex-shaped particles by bonding a group of spheres together [23–27].

The idea of the MCM is to bond a number of spheres to best-fit the surface profile of a 3D irregular particle. According to different requirements, the component spheres can be bonded with no overlaps or with large overlaps. A cluster formed with no overlaps between the component spheres is referred to as an “agglomerate”, which has been widely used for particle crushing simulations [28–32]. Alternatively, the component spheres can be also bonded with large overlaps as a rigid clump to represent an uncrushable particle, and this method is called the overlapping multisphere clump method (OMCM) [24, 25]. Comparing with the modified DEM incorporating particle shape effect, OMCM retains the conventional contact detection algorithm and the practical calculations for contact statics of component spheres within the clumps, thereby ensuring the wide applicability of the conventional DEM simulations. More significantly, OMCM is capable of modeling natural sand particles with extremely complex shapes such as concave shapes. For these reasons, OMCM has become a pragmatic and robust method for many researchers to investigate the particle shape effect by using the conventional DEM.

Two key issues need to be addressed for OMCM. The first is to propose an optimized algorithm to adjust the positions and radii of the component spheres with a limited number inside a clump to best-fit a realistic particle shape. In this regard, several algorithms for OMCM have been proposed, e.g., burn algorithm [20], sphere filling algorithm [24], modified greedy heuristic algorithm [27], etc. The second issue is to eliminate the influence of the incorrect mass and inertia moments of the clump induced by the inhomogeneous overlaps of the filling spheres. For this reason, Ferrellec and McDowell [25] attempted to carefully modify the density of each filling sphere to reach an approximately uniform den-

sity of the generated clump. However, the modified mass and inertia moments of the clump were still not capable to meet the accuracy requirements of the calculation of the particle kinematics in DEM simulations. Therefore, an important aim of this study was to develop an optimized algorithm for OMCM following the idea of Ferrellec and McDowell [25], and further calibrate the mass and inertia moments of the generated clump.

The core objective of this study was to propose a novel framework for the generation of realistic-shaped particles of natural sands in DEM simulations. This framework mainly involved  $\mu$ CT scanning of natural sand particles, image processing of  $\mu$ CT images, SH reconstruction of realistic particle surfaces, random generation of realistic-shaped particles and clump generation by OMCM within an open source DEM LIGGGHTS [33]. Finally, to validate the effectiveness of the generation framework, a series of numerical direct shear tests were performed on a realistic-shaped clump sample and a spherical particle sample. Based on the simulation results, we detailedly explained the differences of the macroscopic and microscopic mechanical behaviors of granular sands affected by realistic particle shapes.

## 2 Representation of realistic particle shapes

### 2.1 $\mu$ CT scanning and image processing

A typical quartz sand, named Leighton Buzzard sand (LBS), was chosen as the research object in this study. As shown by the microscopic view of a typical particle in Fig. 1a, LBS particles always feature a round shape and smooth surface, which may be due to the natural grinding process involved in its chronic geological transportation. To conduct  $\mu$ CT scanning, about 100 LBS particles were randomly chosen from the screening packing, with particle sizes from 1.18 to 2.36 mm. These sand particles were then fixed in a polycarbonate microtube with silicon oil, as shown in Fig. 1b. A Carl Zeiss CT system (METROTOM 1500), provided by the Shenzhen Meixin Testing Technology Co., Ltd., was used to conduct high-resolution x-ray  $\mu$ CT scanning of the LBS specimen. The voxel size of the obtained  $\mu$ CT images was 32.65  $\mu$ m.

To separate contacted sand particles and obtain the shape information of each individual particle, it was necessary to put the obtained  $\mu$ CT images through a series of image processing techniques. Firstly, the solid phases (i.e., sand particles) were distinguished from the void and silicon grease using a thresholding algorithm, and binary  $\mu$ CT images were obtained with the solid pixel being white and background pixel being black. A 3D median filter with an intensity level of 5 pixels was then used to reduce noise within all of the binary  $\mu$ CT images. To separate the contacted particles, a

**Fig. 1** **a** Microscopic view of a typical LBS particle, and **b** LBS particles fixed in a microtube filled with silicon oil

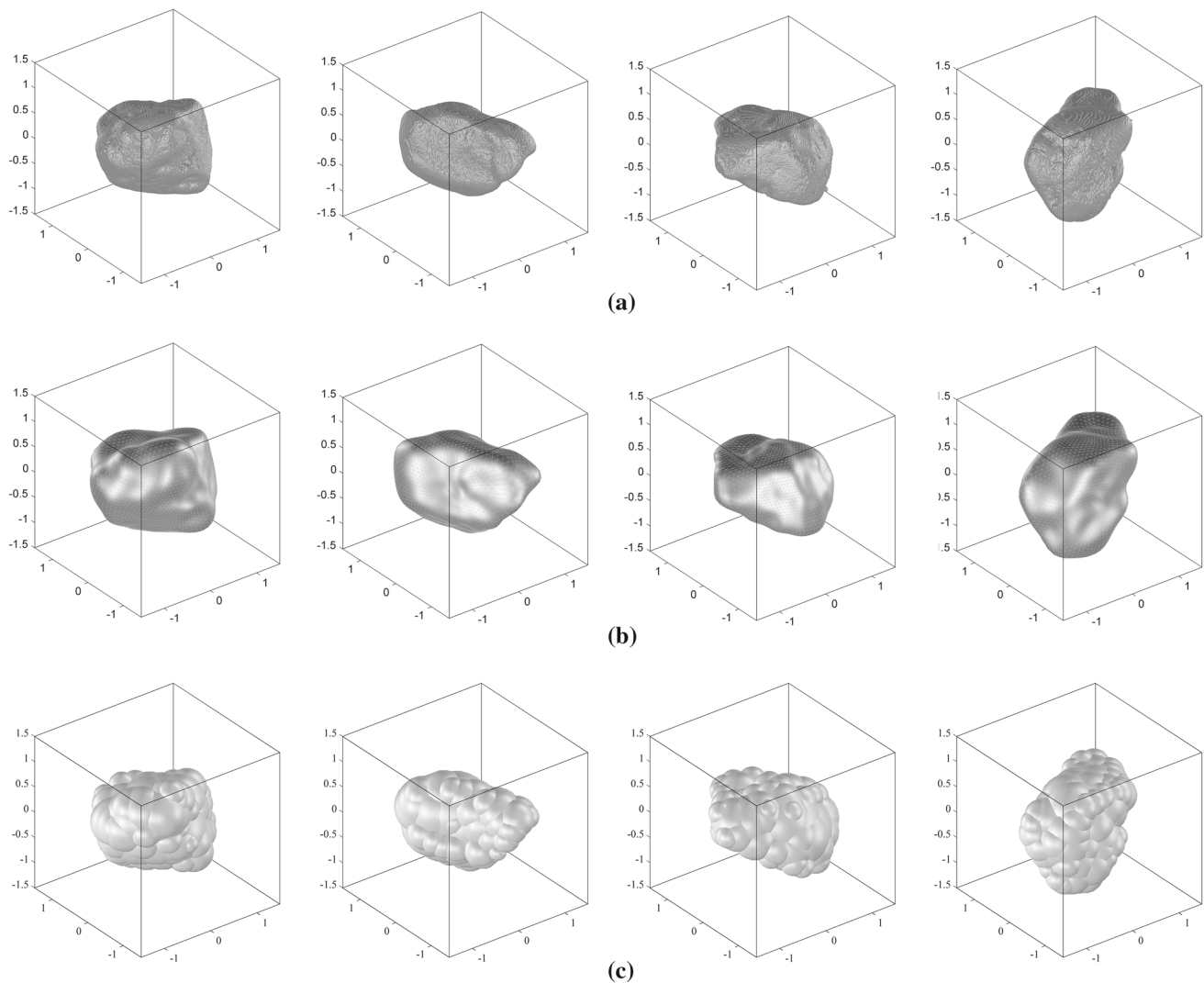
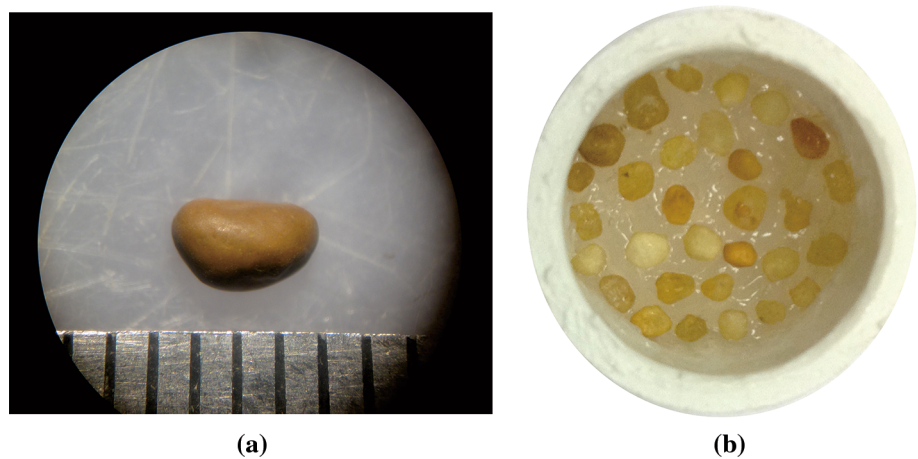


**Fig. 2** **a**  $\mu$ CT images of four scanned particles, **b** SH-reconstructed surfaces of the four particles, and **c** clump representations of the four particles

3D watershed algorithm was applied to the 3D  $\mu$ CT images to prevent over-segmentation. Finally, the individual particles were separated and labeled with different grey levels

using a simple segmentation algorithm. For illustration, the  $\mu$ CT images of four scanned sand particles were visualized in Fig. 2a.

## 2.2 Spherical harmonic reconstruction of particle surface

To implement OMCM, the requisite prior step is to reconstruct the realistic surface of a given sand particle based on its  $\mu$ CT images. In this study, we proposed to reconstruct the particle surface by SH analysis, which has been proven to constitute a powerful tool to represent particle shape features at multiple scale levels [17, 19]. According to previous findings by the authors, the SH-reconstructed surface offers three major advantages [17, 19]: (1) it is a progressive accumulation of surface textures; (2) it is a global optimization to minimize the error to the original particle surface; and (3) it has the characteristics of the SH function, including continuity and smoothness. In particular, the last advantage of the SH-reconstructed surface is critical to implement OMCM successfully. For completeness, the relevant SH theories were briefly introduced below.

After the image processing of the  $\mu$ CT images, the component voxels of a given particle could be easily identified by their labeled grey level. The intrinsic function *bwperim* in MATLAB [34] was utilized to detect the boundary voxels of this particle. According to the spatial positions of the boundary voxels and the voxel resolution (i.e., the spatial width of a voxel), a set of boundary vertices around the particle profile can be accurately positioned by a set of Cartesian coordinates  $\mathbf{V}(x, y, z)$ . As expressed in Eq. (1), the first step of SH analysis is to expand the polar radius from a unit sphere to the particle surface composed of the boundary vertices  $\mathbf{V}(x, y, z)$ , and to calculate the associated SH coefficients:

$$r(\theta, \varphi) = \sum_{n=0}^{\infty} \sum_{m=-n}^n a_n^m Y_n^m(\theta, \varphi) \tag{1}$$

where  $r(\theta, \varphi)$  is the polar radius from the particle center with the spherical coordinates  $\theta \in [0, \pi]$  and  $\varphi \in [0, 2\pi]$ , which can be obtained by the Cartesian-to-spherical coordinate conversion from  $\mathbf{V}(x, y, z)$ ;  $Y_n^m(\theta, \varphi)$  is the SH series given by Eq. (2); and  $a_n^m$  is the associated SH coefficient that needs to be determined.

$$Y_n^m(\theta, \varphi) = \sqrt{\frac{(2n+1)(n-m)!}{4\pi(n+m)!}} P_n^m(\cos \theta) e^{im\varphi} \tag{2}$$

where  $P_n^m(x)$  are the associated Legendre polynomials; and  $n$  and  $m$  are the degree and order of  $P_n^m(x)$ , respectively.

Taking  $r(\theta, \varphi)$  as the input on the left side of Eq. (1), a linear system of equations was obtained with  $(n+1)^2$  unknowns. In this study,  $n_{max}$  was initially set to 15. This value has been shown to be adequate for the reconstruction of concrete aggregates and natural sand particles [17]. Adopting the standard least squares estimation, it is easy to solve these linear equations and determine the optimized solution of  $a_n^m$ .

By using the obtained  $a_n^m$ , it is possible to reconstruct the realistic particle surface by using the following equation:

$$\hat{r}(\theta, \varphi) = \sum_{n=0}^{n_{max}} \sum_{m=-n}^n a_n^m Y_n^m(\theta, \varphi) \tag{3}$$

Figure 2b shows the corresponding SH-reconstructed surfaces of sand particles in Fig. 2a with the SH degree of 15. By visual inspection, it is clear that the shape features of the SH-reconstructed surface agree well with the  $\mu$ CT images of the particle, and further retain the smooth and continuous characteristics of the natural particle surface.

## 3 Overlapping multisphere clump method

### 3.1 Particle shape rebuilding

In this study, we used the sphere filling algorithm proposed by Ferrellec and McDowell [24] to rebuild the realistic particle shape in the DEM framework. As illustrated by Fig. 3a, the major steps of this method are briefly introduced as follows:

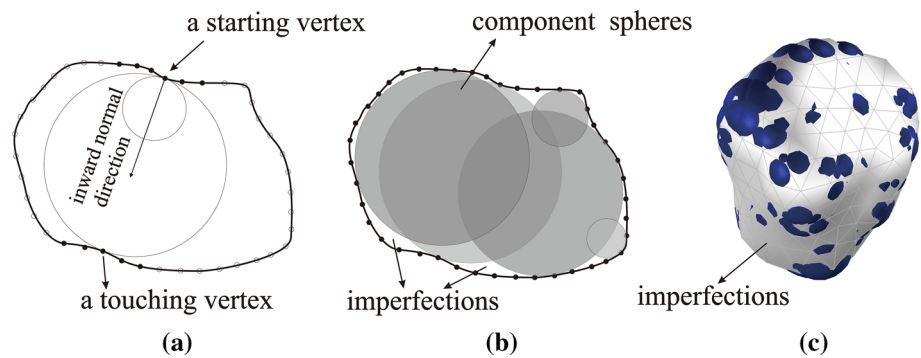
- Step 1 Obtain a series of discrete surface vertices based on the SH-reconstructed surface mesh of a given sand particle.
- Step 2 Randomly choose a vertex, and gradually expand its tangent sphere along its inward normal direction until it touches another boundary vertex on the particle surface. The starting vertex and touching vertex are then excluded from this set of boundary vertices in the following procedures.
- Step 3 Repeat Step 2 by randomly choosing another starting vertex from the rest of the boundary vertices.
- Step 4 Bond the spheres generated by Step 2 and Step 3 as a rigid clump.

During the filling process, three constraints were used to limit the number of generated spheres:

- (1) The distance between the starting vertex of a newly generated sphere and the surface of the existing spheres was measured. If this distance is smaller than a given threshold value  $d_{min}$ , this generated sphere was eliminated because it contributed little to rebuilding the particle shape.
- (2) Generated spheres with a radius smaller than a given value  $r_{min}$  were also eliminated to avoid artificial surface roughness.
- (3) The loop process of Step 3 was ended if the sampling number of the starting vertices was larger than a given percentage  $p_{max}$  of the total vertices.



**Fig. 3** **a** Systematic sketch explaining the selected filling algorithm, **b** geometrical imperfections in 2D, and **c** geometrical imperfections in 3D



Conclusively, the core objective of OMC is to generate the clump precisely representing the particle shape with a limited number of filling spheres. To achieve this aim, it was necessary to determine a set of optimized generation parameters (i.e.,  $d_{min}$ ,  $r_{min}$ , and  $p_{max}$ ) in advance. Ferrellec and McDowell [24] suggested to set low values of  $d_{min}$  and  $r_{min}$ , and a high value of  $p_{max}$ . However, it is still not clear how to determine optimized parameters according to the requirement of accuracy of the clump and the number of filling spheres. Based on a series of empirical trials, Table 1 presented three sets of adequate parameters for OMC, and Fig. 4 displayed the SH reconstruction of a typical sand particle (i.e., Fig. 4a) and its generated clumps (i.e., Fig. 4b–d) with these sets of parameters. By visual inspection, it is clear that the shape features of the clump gradually approach the real sand particle with the increased number of filling spheres. However, the volume imperfection between the clump and the real sand particle was still inevitable by using OMC, as illustrated in Fig. 3b, c. Moreover, the inaccuracy of the mass and inertia moments of the clump, induced by the high overlapping of the filling spheres, may result in incorrect kinematic behaviors of the clumps in DEM simulations. For these reasons, the following section will further investigate the accuracy of the clump representing the volume, mass, and inertia moments of the sand particle to validate the effectiveness of OMC with the given parameters in Table 1.

### 3.2 Particle volume and inertia moments

Traditionally, the volume, mass, and inertia moments of the clump were determined by a conventional clump logic used by many DEM codes such as PFC<sup>3D</sup> [35]. However, recent studies proved that this logic is not suitable for the clump generated by OMC, because the double counting and the heterogeneity of density within the overlapping volume will result in inaccurate mass and inertia moments of the clump [25, 27, 36]. To overcome this problem, we introduced a probabilistic method to calculate the kinematic properties of the clump, including the mass and inertia moments. The core idea of this method is to utilize the Monte Carlo simulation

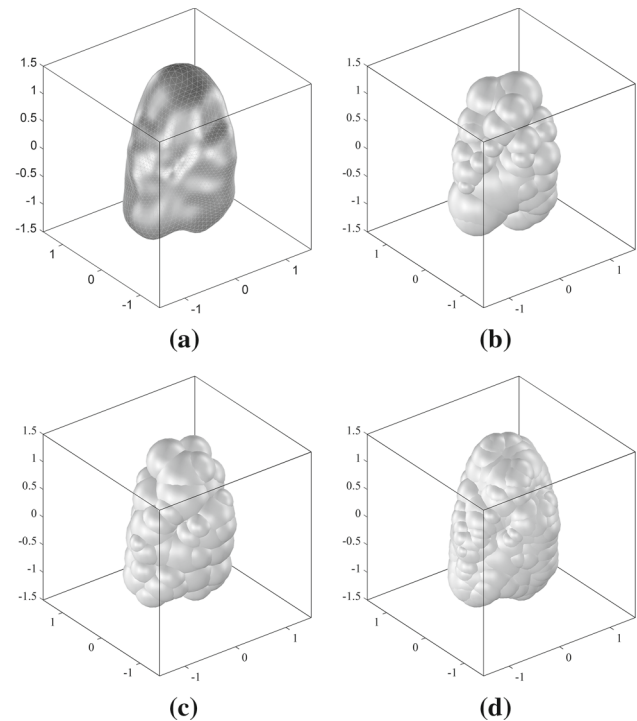


**Fig. 4** **a** SH reconstruction of a typical sand particle, **b** clump generated with the first set of parameters in Table 1, **c** clump generated with the second set of parameters in Table 1, and **d** clump generated with the third set of parameters in Table 1

within the volume of the clump, and then evaluate the integral expressions for its kinematic properties. Similar method was also used by Alonso-Marroquín and Wang [37] to determine the kinematic properties of spheropolygons. Firstly, a bounding box with the principal dimensions of a given multisphere clump was generated, as illustrated in Fig. 5a. A large number (e.g.,  $N = 10,000$ ) of points were then randomly generated within this bounding box. The points with the number of  $n$  inside the clump volume were reserved, as demonstrated by the red point in Fig. 5b. According to the theory of the Monte Carlo simulation, the volume of the clump  $V$  can be obtained by:

**Table 1** Relative deviations of the volume and inertia moments using different sets of parameters

Constraint generation parameters			Relative deviation of volume (%)	Relative deviation of PMI (%)	Average number of component spheres
$d_{min}$ (mm)	$r_{min}$ (mm)	$p_{max}$ (%)			
<i>μCT-scanned sand particles</i>					
0.04	0.1	80	14.5	16.8	16
0.03	0.08	90	8.7	10.1	30
0.02	0.04	95	1.9	2.1	67
<i>Virtual sand sample</i>					
0.03	0.08	90	8.0	9.7	31

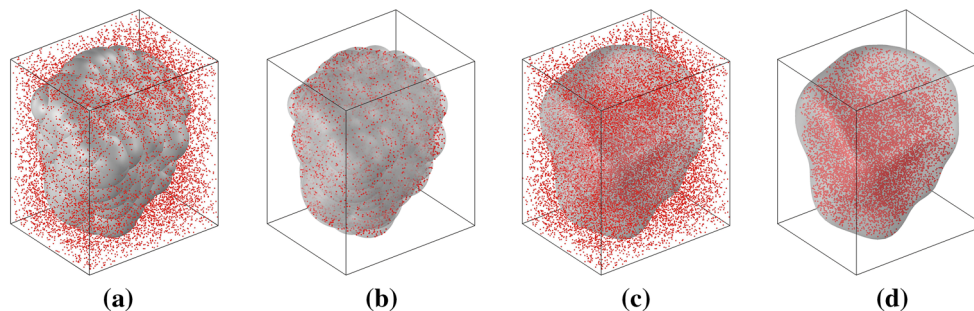


**Fig. 5** Schematic diagram of Monte Carlo simulation, **a** points randomly scattered into the bounding box, **b** points fall inside the clump were reserved, **c** points randomly scattered into the bounding box of a SH particle, and **d** points fall inside the SH particle were reserved

$$V = \frac{n}{N} V_{box} \tag{4}$$

where  $V_{box}$  is the volume of the bounding box. Therefore, the mass of the clump  $m$  can be easily obtained by the product of  $V$  and a given material density of the particle. To further calculate the inertia moments, each remaining point  $(x_i^p, x_j^p, x_k^p)$  was assigned a micro mass  $m/n$ . Therefore, the mass center  $(x_i, x_j, x_k)$ , moments, and products of inertia  $I_{ii}$  and  $I_{ij}$  of a clump can be calculated by the following equations:

$$x_i = \frac{1}{n} \sum_{p=1}^n x_i^p \tag{5}$$

$$I_{ii} = \frac{m}{n} \sum_{p=1}^n \left\{ (x_j^p - x_j)^2 + (x_k^p - x_k)^2 \right\} \tag{6}$$

$$I_{ij} = \frac{m}{n} \sum_{p=1}^n \left\{ -(x_i^p - x_i)(x_j^p - x_j) \right\} \quad (j \neq i) \tag{7}$$

The above method can also be extended to calculate the volume, mass, and inertia moments of the SH-reconstructed sand particle, as illustrated by Fig. 5c and 5d. By using the proposed calculation method, Table 1 summarized the average deviations of the volume and three principal moments of

inertia (PMI) between the SH reconstruction and the clump generated by different sets of generation parameters for all of the sand particles. The average numbers of filling spheres within the clump were also included in this table. It is clearly noted that the deviation of the volume and PMI dramatically decreases with the decrease of  $d_{min}$  and  $r_{min}$ , and the increase of  $p_{max}$ , whereas the number of filling spheres apparently increases. Considering the computational efficiency of the DEM simulation, the second set of generation parameters in Table 1 was finally selected in this study. The generated clumps had an average number of 30 component spheres, and average deviations of 8.7 and 10.1% in volume and PMI, respectively. Figure 2c shows the generated clumps with this set of generation parameters, which agrees well with the shape features of their corresponding sand particles in Fig. 2a.

### 4 Specimen generation and direct shear testing

To further demonstrate the particle shape effect on the mechanical properties of granular sands, a series of numerical direct shear tests were conducted in this section. Due to the limited number of μCT-scanned sand particles, it is difficult to generate a numerical sample with a large number of realistic-shaped particles. Consequently, the authors

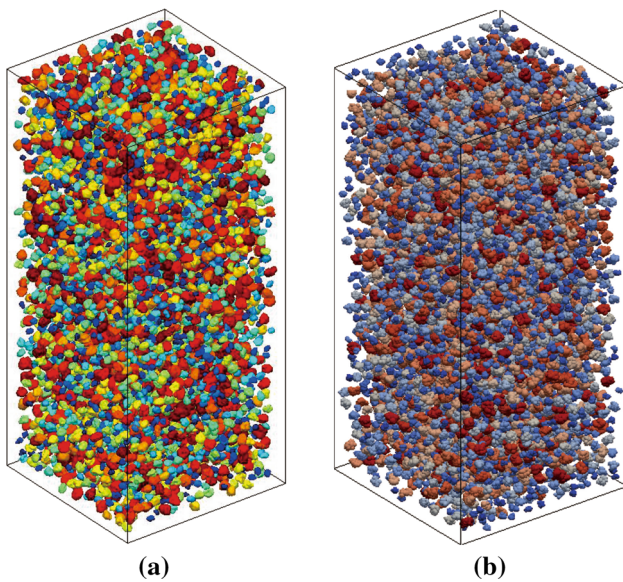


**Fig. 6** **a** Virtual sand particle assembly generated from expanding process, and **b** corresponding clump assembly

proposed a statistical approach for generating a virtual sand assembly composed of a large number of realistic-shaped particles, but retaining the major shape features of natural sand [18]. By employing this approach, a virtual sand assembly containing 6500 realistic-shaped particles with a uniform particle size distribution from 1 to 2 mm was generated in a rectangular box with the dimensions of 25 mm × 25 mm × 60 mm, as visualized in Fig. 6a. By using the same set of generation parameters in Sect. 3, OCMC was applied for each individual particle to rebuild a corresponding DEM-oriented clump in the box, and the obtained clump sample was visualized in Fig. 6b. The average number of filling spheres and deviations of the volume and PMI of all the clumps were also summarized in Table 1, which were basically acceptable for the DEM simulations.

In accordance with the dimensions of the rectangular box for the generation of the sand assembly, a direct shear box was generated by placing six rigid walls, including four lateral walls and two horizontal walls, as illustrated in Fig. 7a. The hertz contact theory [38] was adopted to define the constitutive response of the inter-particle contacts and wall-particle contacts, in which the major DEM parameters were summarized in Table 2. It should be noted that the wall element was set as the granular wall that can be regarded as the surface of a sphere with infinite mass and radius. Therefore, the contact parameters and the constitutive response of the inter-particle contacts and wall-particle contacts are all the same. To consolidate the sample to a dense state, the initial friction coefficient of the particles was set to zero, and the upper wall and the lower wall moved towards each other at a constant speed until the vertical stress of the sample

**Table 2** Major DEM parameters selected in this study

Parameter	Value
Size range (mm)	1–2
Density (g/cm <sup>3</sup> )	2.6
Total mass of the sample (g)	18.29
Young's modulus (Pa)	$5 \times 10^7$
Poisson ratio	0.15
Restitution coefficient	0.3
Friction coefficient	0.4

reached a given confining stress (i.e., 25, 50, 75, and 100 kPa) (see Fig. 7b). As a contrast, a conventional spherical particle sample with the same particle size distribution as the clump sample was generated to demonstrate the shape effect on the mechanical behaviors of the samples. Figure 8 shows the initial void ratios of these two samples subjected to different consolidation stresses. For both samples, the initial void ratio apparently decreases with the increase of consolidation stress. It can be noted that the clump sample has a higher void ratio than the sphere sample under the same consolidation stress. Moreover, the irregular form and angular corners of the realistic-shaped clumps can highly resist the rearrangement of the particles under the consolidation, which results in large voids between the particles.

After the consolidation of the sample, the inter-particle friction coefficient was reset to 0.4, and the side walls were cut horizontally into two equal halves by an imaginary shear plane passing through the middle of the specimen. To prevent the particles from escaping during the shear process, two horizontal wings were placed between the upper and lower halves of the shear box, as demonstrated in Fig. 7c [39]. The shear process was then performed by moving these two halves relative to each other at a constant velocity of 1 mm/s. In order to balance computational efficiency and accuracy, the time step was chosen as  $8 \times 10^{-7}$  s, which is one-tenth of the critical Rayleigh time [38, 40]. During the whole shear process, the vertical stress of the sample was maintained constant under a servo control, and the shear stress, shear displacement, and volume change of the sample were mainly monitored. Specifically, the volume of the lower half box remained a constant during the shear process, while the volume of the upper half box updated according to the position of the upper horizontal wall determined by the servo control. Therefore, the volume change of the sample is the difference between the updated volume and the initial volume of the upper half box. Figure 7d shows the final state of the sample subjected to the shear displacement ratio of 20%, which was defined by the ratio of the shear displacement to the width of the shear box.

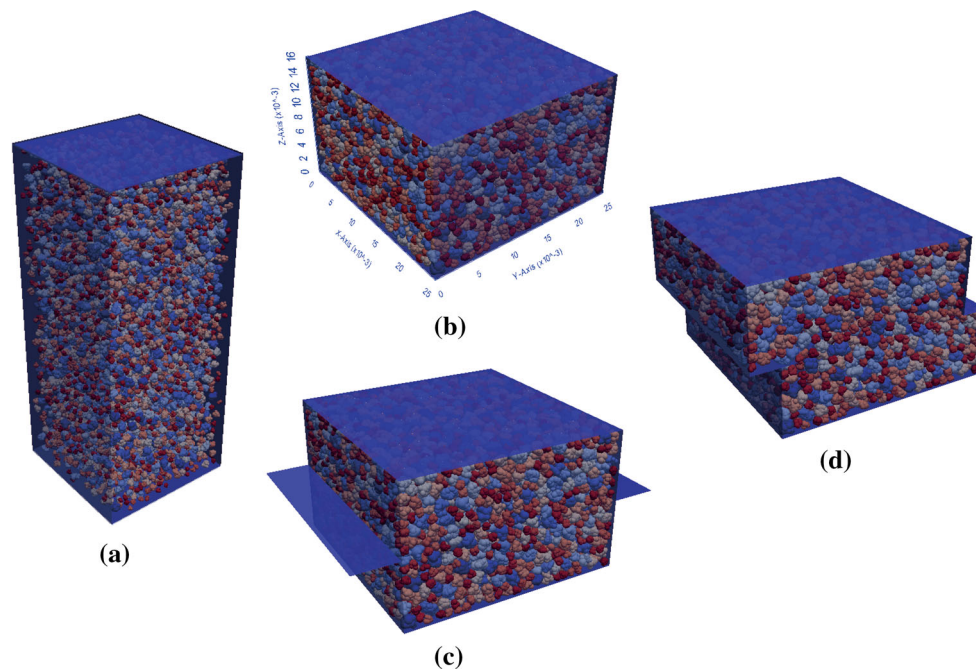


**Fig. 7** Schematic diagram of specimen generation and shear process, **a** particles generated in the shear box (before being compacted), **b** a compacted specimen generated, **c** wings attached and specimen is ready to shear, and **d** final state of the shear process

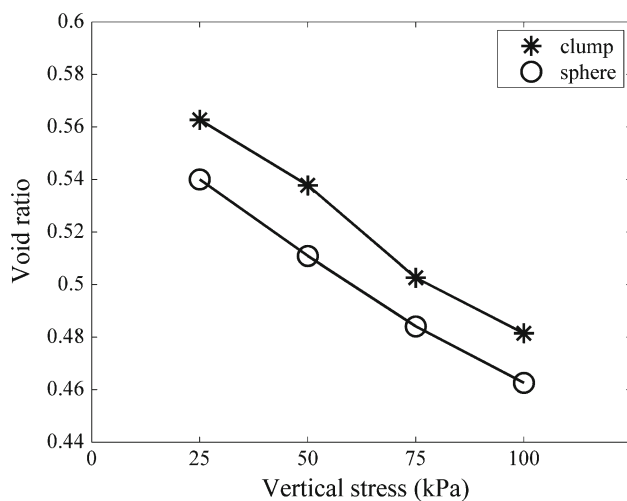


**Fig. 8** Initial void ratio under different vertical stresses

## 5 Results and discussion

### 5.1 Macroscopic mechanical response

Based on a series of numerical direct shear tests, Fig. 9 shows the shear stress and volume change as functions of the shear displacement ratio for both samples. Due to the dense state of the sample, a clear peak and subsequent softening-behavior can be observed in all of the stress-displacement curves (see Fig. 9a), and a remarkable shear-induced dilation can be

found in all of the dilation-displacement curves (see Fig. 9b). The peak stress, residual stress, and volumetric dilation of both samples apparently increase with the increase of vertical stress. With regard to the shape effect, as expected, the clump sample has a much higher peak stress, residual stress, and volumetric dilation than the sphere sample under the same vertical stress. These well-known results clearly prove the importance of realistic particle shapes in DEM simulations, and the effectiveness of the proposed framework for the generation of realistic particle shapes.

To further analyze the effect of the particle shape on the bulk friction angle of the sample, Fig. 10 plots a scatter diagram of the peak and residual shear stress against the vertical stress for all of the samples, and the linear fitting curves are also included. The bulk friction angle can be determined by the slope of the fitting curve according to Mohr–Coulomb criteria. The peak bulk friction angles of the clump and sphere samples are  $52^\circ$  and  $40^\circ$ , respectively. The residual friction angles of clump and sphere samples are  $43^\circ$  and  $37^\circ$ , respectively. This demonstrates that the incorporation of the realistic particle shape brings a major increase of the bulk friction angle of the sample at peak state (i.e.,  $12^\circ$ ) and a minor increase of the bulk friction angle of the sample at residual state (i.e.,  $6^\circ$ ) due to the high interlocking between the shaped particles. This difference indicates that the particle shape effect is more remarkable at the peak state, which might be attributable to a weakening of the interlocking force within the shear band at the residual state.



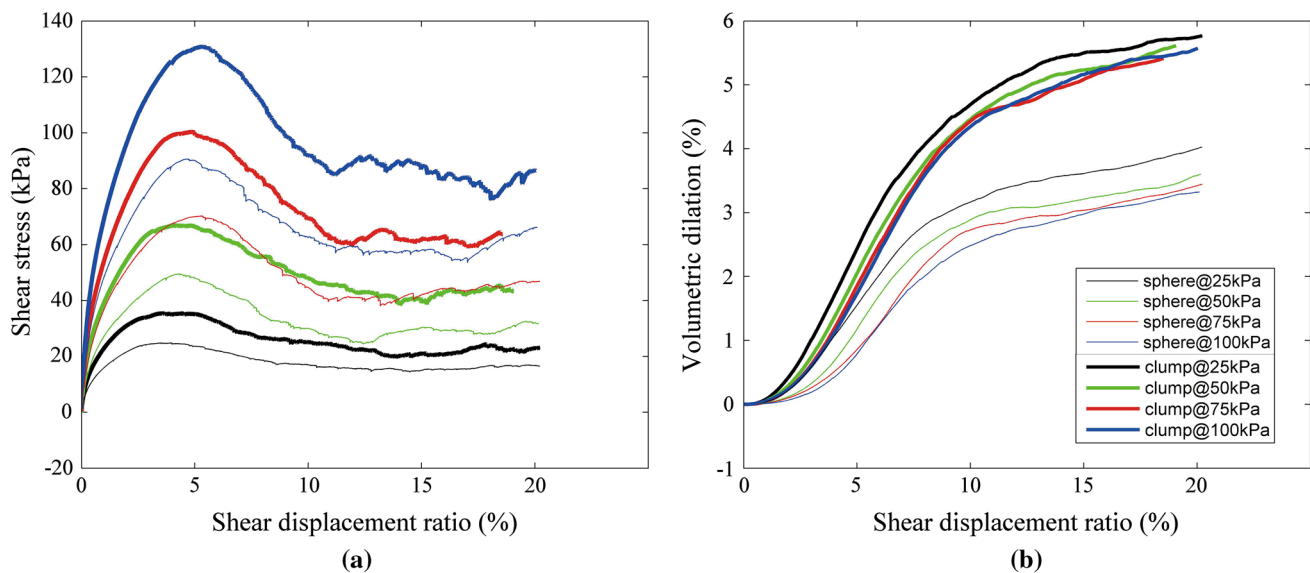


**Fig. 9** Macro shear behavior comparison, **a** shear stress—shear displacement ratio curves, and **b** volumetric dilation—shear displacement ratio curves

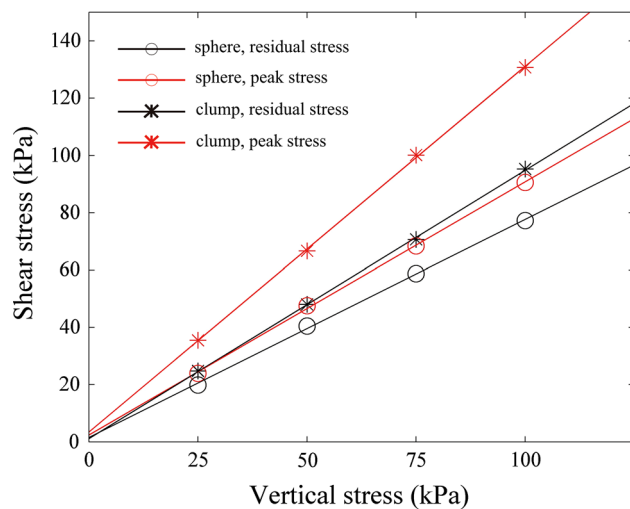


**Fig. 10** Peak and residual shear stress versus incremental vertical stresses

## 5.2 Micromechanics of sand particles

To gain insight into the micromechanics of the particles, Fig. 11 shows 5 snapshots (corresponding to before shear state, 5, 10, 15% shear displacement ratio states and final shear state) of the strong normal contact force network and polar distributions of these two samples under the vertical stress of 50 kPa during the shearing process. The top 20% of contact forces within the sample were defined as the strong contact force in this study. After the equilibrium of the consolidation, a clear vertical pattern of the strong force chains can be observed to resist the vertical consolidation stress, and the principal direction of the polar distribution of the strong

forces can be found to be vertical, as well. With the development of the shearing, the major pattern of the strong force chains and the principal direction of the polar distribution firstly rotates along the shearing direction before the peak state, and then remains stable at the residual state. It was also found that the anisotropic intensity of the strong contact forces dramatically increased before the peak state, and then slightly decreased to a stable magnitude at the residual state. It is worth noting that the anisotropic intensity of the strong contact forces of the clump sample was slightly weaker than that of the sphere sample, especially at the peak state. This interesting phenomenon may be due to the inhibiting effect of the strong interlocking between the realistic-shaped particles on the development of the shear-induced anisotropy of the clump sample.

In order to quantify the interlocking effect at an inter-particle contact, a friction mobilization index  $I_m$  [41] was introduced in this study, which was defined by the ratio of the tangential force  $f_t$  to the maximum anti-sliding force  $\mu f_n$  of this contact. Figure 12a shows the evolution of average  $I_m$  of all of the inter-particle contacts within both samples during the shearing process. In addition to no remarkable peak, a similar pattern with the stress-displacement curves (see Fig. 9a) can be observed herein. Moreover, the fluctuation of the  $I_m$  curves was mainly attributable to the slip-stick mechanism in the quasi-static shearing, a phenomenon that was also previously found by the authors [9] and other researchers [42]. By carefully examining this figure, two sets of  $I_m$  curves can be distinguished, which means that the stress level has no apparent influence on the inter-particle interlocking. Specifically, the clump sample has a much higher  $I_m$  than the sphere sample at the same vertical stress, which indicates that

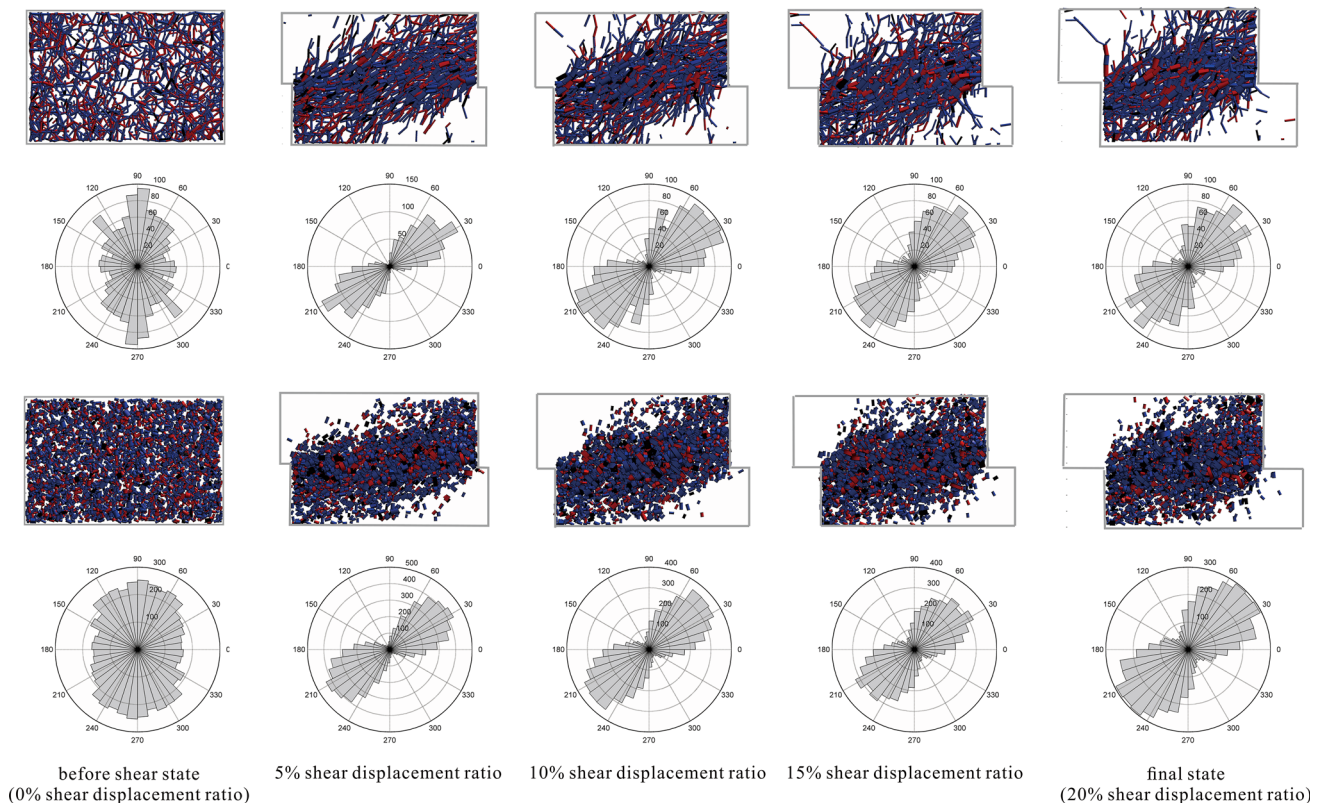


Fig. 11 Side view and anisotropy of strong contact force chains

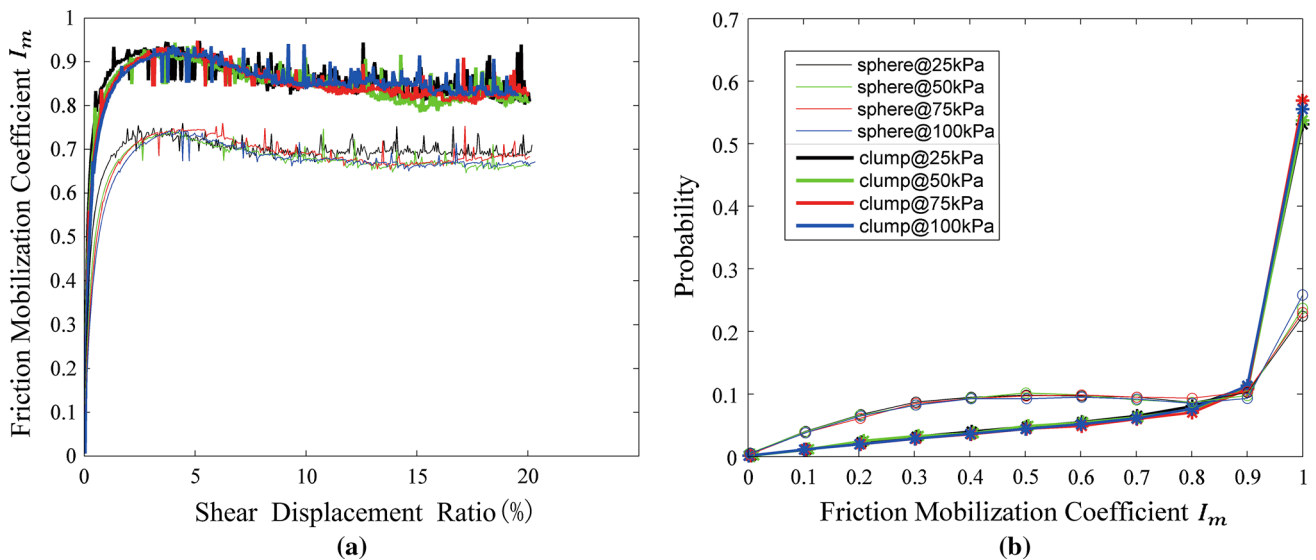


Fig. 12 **a** Probability distribution profiles of friction mobilization coefficient at peak state, and **b** evolution of average friction mobilization coefficient during the shear process

the realistic particle shape highly enhances the inter-particle interlocking at the particle-scale level.

Figure 12b presents the probability distributions of  $I_m$  for both samples at the peak state. It is interesting to find that the distribution profiles of the clump samples exhibit remarkable

differences from those of the sphere samples. Specifically, the former shows a nearly linear increase of probability from  $I_m = 0$  to  $I_m = 0.9$  and an extremely high probability at  $I_m = 1$ , while the later approximates a constant probability from  $I_m = 0.3$  to  $I_m = 0.9$  and a relatively low probability at  $I_m = 1$ .

The higher probability at  $I_m = 1$  for the clump samples indicates that a greater proportion of the inter-particle contacts is bearing its maximum capacity of the sliding resistance, contributing to the enhancement of the shear resistance of the samples. These findings can reveal the micromechanics of interlocking between the realistic-shaped particles.

## 6 Conclusions

The major contribution of this study was to propose a novel framework for the generation of realistic-shaped particles of natural sands in 3D DEM simulations. The generation framework mainly involved  $\mu$ CT scanning of the sand particles, image processing of  $\mu$ CT images, SH reconstruction of particle surfaces, random generation of realistic-shaped particles, and implementation of OMCM within an open source DEM LIGGGHTS. In order to validate the accuracy of OMCM and calibrate the kinematic properties of the generated clump, the mass and inertia moments of the clump were precisely investigated by using the Monte Carlo method. The results demonstrated that the clump with a limited number of filling spheres generated by OMCM with optimized generation parameters was sufficient to represent the volume, mass, and inertia moments of realistic sand particles.

By using the generation framework, a series of numerical direct shear tests were performed to demonstrate the significant effect of the realistic particle shape on the macroscopic and microscopic mechanical behaviors of granular sands. The simulation results demonstrated that the realistic shape highly increases the inter-particle interlocking rather than the anisotropic intensity of strong contact force chains, in turn enhancing the shear resistance and the shear-induced dilation of the sands. At the particle scale level, it was further shown that the inter-particle contacts of the clump sample have higher friction mobilization than that of the sphere sample. This finding revealed the interlocking mechanism enhanced by the particle shape at the microscopic level. Moreover, all the simulation results proved the effectiveness of the proposed framework for generating realistic particle shapes within DEM simulations. Based on the present work, our future research will generate realistic-shaped particles with more sophisticated shape features of natural sands, and quantify the correlation between the statistics of the shape parameters (e.g., sphericity, roundness, convexity, aspect ratio etc.) [43] and the microscopic and macroscopic mechanical properties of natural sands.

## Compliance with ethical standards

**Conflict of interest** The authors declare that there is no conflict of interest.

## References

- Guo, P., Su, X.: Shear strength, interparticle locking, and dilatancy of granular materials. *Can. Geotech. J.* **44**(5), 579–591 (2007)
- Tsomokos, A., Georgiannou, V.: Effect of grain shape and angularity on the undrained response of fine sands. *Can. Geotech. J.* **47**(5), 539–551 (2010)
- Lin, X., Ng, T.-T.: A three-dimensional discrete element model using arrays of ellipsoids. *Geotechnique* **47**(2), 319–329 (1997)
- Nouguier-Lehon, C., Cambou, B., Vincens, E.: Influence of particle shape and angularity on the behaviour of granular materials: a numerical analysis. *Int. J. Numer. Anal. Method Geomech.* **27**(14), 1207–1226 (2003)
- Zhou, Z., Zou, R., Pinson, D., Yu, A.: Angle of repose and stress distribution of sandpiles formed with ellipsoidal particles. *Granul. Matter* **16**(5), 695–709 (2014)
- Zhao, S., Zhou, X., Liu, W.: Discrete element simulations of direct shear tests with particle angularity effect. *Granul. Matter* **17**(6), 793–806 (2015)
- Iwashita, K., Oda, M.: Micro-deformation mechanism of shear banding process based on modified distinct element method. *Powder Technol.* **109**(1), 192–205 (2000)
- Jiang, M., Yu, H.-S., Harris, D.: A novel discrete model for granular material incorporating rolling resistance. *Comput. Geotech.* **32**(5), 340–357 (2005)
- Zhou, B., Huang, R., Wang, H., Wang, J.: DEM investigation of particle anti-rotation effects on the micromechanical response of granular materials. *Granul. Matter* **15**(3), 315–326 (2013)
- Azéma, E., Radjai, F., Dubois, F.: Packings of irregular polyhedral particles: strength, structure, and effects of angularity. *Phys. Rev. E* **87**(6), 062203 (2013)
- Nassauer, B., Kuna, M.: Contact forces of polyhedral particles in discrete element method. *Granul. Matter* **15**(3), 349–355 (2013)
- Nassauer, B., Liedke, T., Kuna, M.: Polyhedral particles for the discrete element method. *Granul. Matter* **15**(1), 85–93 (2013)
- Pournin, L., Weber, M., Tsukahara, M., Ferrez, J.-A., Ramaioli, M., Liebling, T.M.: Three-dimensional distinct element simulation of spherocylinder crystallization. *Granul. Matter* **7**(2–3), 119–126 (2005)
- Houlsby, G.: Potential particles: a method for modelling non-circular particles in DEM. *Comput. Geotech.* **36**(6), 953–959 (2009)
- Boon, C.W., Houlsby, G., Utili, S.: A new contact detection algorithm for three-dimensional non-spherical particles. *Powder Technol.* **248**, 94–102 (2013)
- Garboczi, E.J.: Three-dimensional mathematical analysis of particle shape using X-ray tomography and spherical harmonics: application to aggregates used in concrete. *Cem. Concr. Res.* **32**(10), 1621–1638 (2002)
- Zhou, B., Wang, J., Zhao, B.: Micromorphology characterization and reconstruction of sand particles using micro X-ray tomography and spherical harmonics. *Eng. Geol.* **184**, 126–137 (2015)
- Zhou, B., Wang, J.: Random generation of natural sand assembly using micro x-ray tomography and spherical harmonics. *Géotech. Lett.* **5**(1), 6–11 (2015)
- Zhou, B., Wang, J.: Generation of a realistic 3D sand assembly using X-ray micro-computed tomography and spherical harmonic-based principal component analysis. *Int. J. Numer. Anal. Method Geomech.* **41**(1), 93–109 (2017)
- Wang, L., Park, J., Fu, Y.: Representation of real particles for DEM simulation using X-ray tomography. *Constr. Build. Mater.* **21**(2), 338–346 (2007)
- Andrade, J.E., Lim, K.-W., Avila, C.F., Vlahinić, I.: Granular element method for computational particle mechanics. *Comput. Methods Appl. Mech. Eng.* **241**, 262–274 (2012)

22. Lim, K.W., Andrade, J.E.: Granular element method for three-dimensional discrete element calculations. *Int. J. Numer. Anal. Method Geomech.* **38**(2), 167–188 (2014)
23. Favier, J., Abbaspour-Fard, M., Kremmer, M.: Modeling nonspherical particles using multisphere discrete elements. *J. Eng. Mech.* **127**(10), 971–977 (2001)
24. Ferrellec, J.-F., McDowell, G.: A simple method to create complex particle shapes for DEM. *Geomech. Geoeng. Int. J.* **3**(3), 211–216 (2008)
25. Ferrellec, J., McDowell, G.: Modelling realistic shape and particle inertia in DEM. *Géotechnique* **60**(3), 227–232 (2010)
26. Garcia, X., Latham, J., Xiang, J., Harrison, J.: A clustered overlapping sphere algorithm to represent real particles in discrete element modelling. *Geotechnique* **59**(9), 779 (2009)
27. Li, C.-Q., Xu, W.-J., Meng, Q.-S.: Multi-sphere approximation of real particles for DEM simulation based on a modified greedy heuristic algorithm. *Powder Technol.* **286**, 478–487 (2015)
28. Cheng, Y., Nakata, Y., Bolton, M.: Discrete element simulation of crushable soil. *Geotechnique* **53**(7), 633–642 (2003)
29. Cheng, Y., Bolton, M., Nakata, Y.: Crushing and plastic deformation of soils simulated using DEM. *Geotechnique* **54**(2), 131–142 (2004)
30. Bolton, M., Nakata, Y., Cheng, Y.: Micro-and macro-mechanical behaviour of DEM crushable materials. *Géotechnique* **58**(6), 471–480 (2008)
31. Wang, J., Yan, H.: DEM analysis of energy dissipation in crushable soils. *Soils Found.* **52**(4), 644–657 (2012)
32. Wang, J., Yan, H.: On the role of particle breakage in the shear failure behavior of granular soils by DEM. *Int. J. Numer. Anal. Method Geomech.* **37**(8), 832–854 (2013)
33. Kloss, C., Goniva, C., Hager, A., Amberger, S., Pirker, S.: Models, algorithms and validation for opensource DEM and CFD-DEM. *Prog. Comput. Fluid Dyn. Int. J.* **12**(2–3), 140–152 (2012)
34. Guide, M.U.s.: The Mathworks. Inc., Natick, MA **5**, 333 (1998)
35. PFC3D, U.s.M.: Itasca Consulting Group. Inc, Minneapolis, USA (2005)
36. Shi, C., Li, D.-J., Xu, W.-Y., Wang, R.: Discrete element cluster modeling of complex mesoscopic particles for use with the particle flow code method. *Granul. Matter* **17**(3), 377–387 (2015)
37. Alonso-Marroquín, F., Wang, Y.: An efficient algorithm for granular dynamics simulations with complex-shaped objects. *Granul. Matter* **11**(5), 317–329 (2009)
38. Di Renzo, A., Di Maio, F.P.: Comparison of contact-force models for the simulation of collisions in DEM-based granular flow codes. *Chem. Eng. Sci.* **59**(3), 525–541 (2004)
39. Ni, Q., Powrie, W., Zhang, X., Harkness, R.: Effect of particle properties on soil behavior: 3-D numerical modeling of shearbox tests. In: *Numerical methods in geotechnical engineering*, pp 58–70 (2000)
40. Li, Y., Xu, Y., Thornton, C.: A comparison of discrete element simulations and experiments for ‘sandpiles’ composed of spherical particles. *Powder Technol.* **160**(3), 219–228 (2005)
41. Azéma, E., Radjaï, F.: Force chains and contact network topology in sheared packings of elongated particles. *Phys. Rev. E* **85**(3), 031303 (2012)
42. Alonso-Marroquín, F., Vardoulakis, I., Herrmann, H., Weatherley, D., Mora, P.: Effect of rolling on dissipation in fault gouges. *Phys. Rev. E* **74**(3), 031306 (2006)
43. Zhou, B., Wang, J., Wang, H.: Three-dimensional sphericity, roundness and fractal dimension of sand particles. *Géotechnique* **68**(1), 18–30 (2018)